Permeability of oolitic limestones from the Upper Rhine Graben

[1]Sarvar Mammadov, [1]Patrick Baud, [1]Michael Heap, [1]Mathieu Schuster, [1]Thierry Reuschlé

[1]Institut Terre et Environnement de Strasbourg, Université de Strasbourg, CNRS UMR 7063, Strasbourg, France

This presentation participates in OSPP

Outstanding Student & PhD candidate Presentation contest

École et observatoire des sciences de la Terre Université de Strasbourg

Ministry of Science and Education Republic of Azerbaijan

1. Introduction

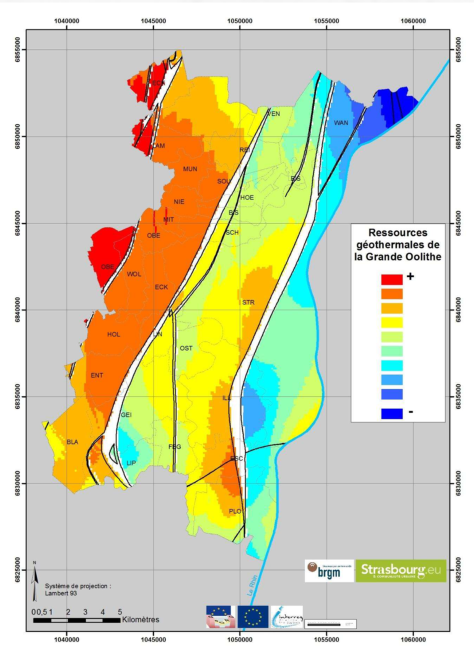

Total heat capacity: 4.1 * 10^{10} GJ
Theoretical available heat quantity: 9.9 * 10^{9} GJ

The Grande Oolithe (GO) is an allochemical limestone from the Middle Jurassic (170.9 – 168.2 Ma) composed of millimetric oolites. The formation can be found in Alsace (north-east of France), locally outcropping in the Rhine Graben, mostly at shallow depths. Several exploration wells were drilled in central and southern Alsace for hydrocarbon exploitation, and it is prospective target for geothermal development. A comprehensive evaluation of the geothermal potential of this formation hinges on a detailed understanding of its mechanical and physical properties, in particular permeability.

Mechanical behavior and fluid flow could be strongly influenced in particular by the degree of cementation and the proportion of macro and micropores in limestones, which often have a dual porosity structure (Zhu et al., 2010).

Previous data reported by BRGM suggest highly variable range of porosity and relatively low permeability which could be enhanced by fracture network (83-SGN-007-ALS., 1982).

Main objectives:

- Determin**e mechanical and physical properties** of Grande Oolithe at in situ conditions;
- Analyze the **pore structure and cementation** in Grande Oolithe and their **effect on the strength**, **development of various failure modes, and fluid flow**;
- Study the **water weakening effect** on Grande Oolithe;

2.1. Materials

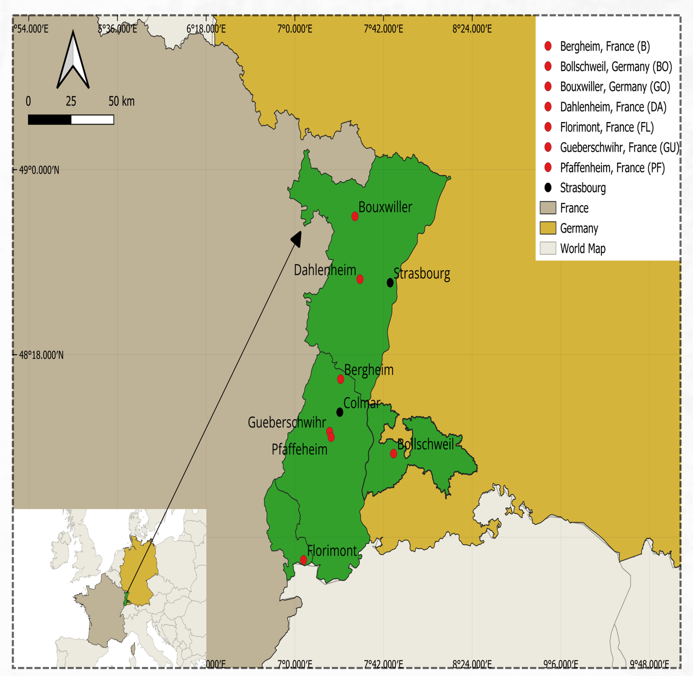

Porosity and permeability were measured prior to deformation on 20 mm x 40 mm sized cylindrical samples taken from 7 outcrops.

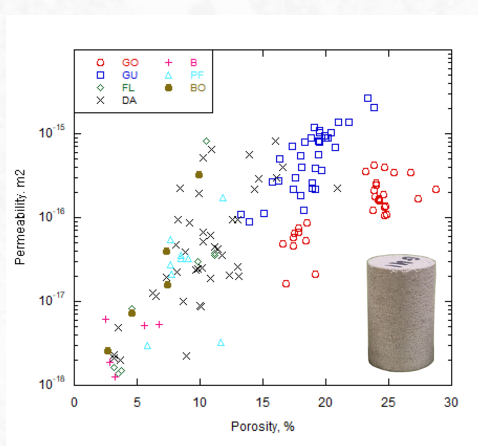

High resolution (11 μm) X-ray CT scans of intact a)GO and b)GU1 samples

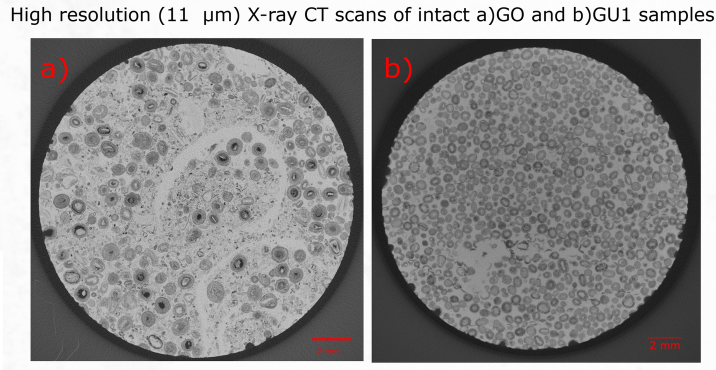

Petrophysical description of porous end-members selected for this study

Rock description	Origin	Mean connected porosity (%)	Mean permeability (m^2)	Mean grain diameter (μm)	Mineralogical composition
GO limestone	Bouxwiller, France	24.8	2.2E-16	856	98.8%: calcite, 0.9% : quartz, 0.3%: kaolinite
GU1 limestone	Gueberschwihr, France	19.4	6.5E-16	617	98.7 %: calcite, 0.9% :gypsum, 0.3%: quartz, 0.1%: kaolinite

2.2. Experimental setup

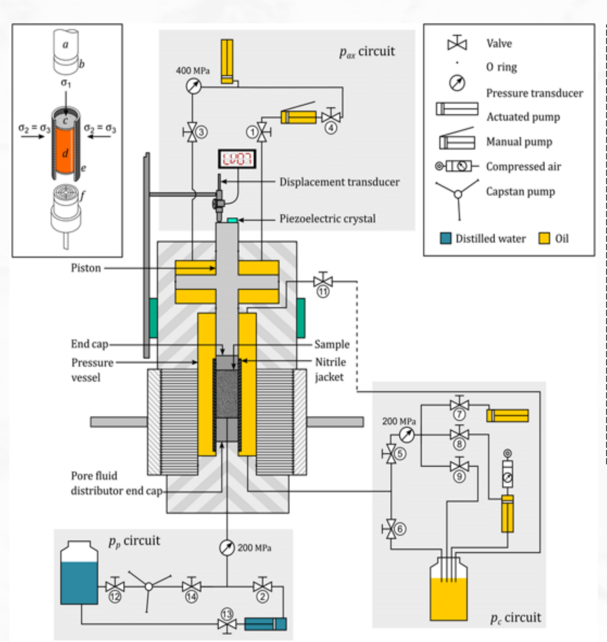

Schematic of triaxial deformation apparatus (Farquharson et al., 2017)

Hydrostatic and conventional triaxial experiments were conducted on dry and saturated samples (at 10 MPa pore pressure) at effective pressures ranging from 5 to 20 MPa for GO (24.8%) and GU1 (19.4%) blocks.

For wet experiments, vacuum-dried (48 h) and saturated samples (deionized water) were deformed under fully drained conditions.

All experiments were conducted at room temperature and a constant strain rate of 10^{-5} s^{-1}.

Permeability of a hydrostatically/triaxially compressed sample was estimated using the steady-state flow method.

Petrographic thin sections were prepared on deformed samples for microstructural analysis using a scanning electron microscope (SEM).

Triaxial loading: $\sigma_1 > \sigma_2 = \sigma_3$

Hydrostatic loading: $\sigma_1 = \sigma_2 = \sigma_3$

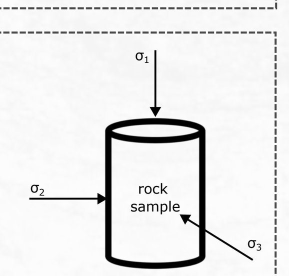

3.1. Mechanical data

The behavior of GO block (φ = 24.8%) was ductile over the entire range of effective pressures with shear-enhanced compaction seen in all cases. Increasing effective pressure leads to an increase in strain hardening. Transition from shear-enhanced compaction to shear-induced dilation was seen at 10 and 15 MPa effective pressure, with porosity reduction of 2.91% and 4.2%, respectively.

For GU1 block (φ = 19.4 %), dilatancy (starting at the critical stress C') and strain softening were observed at an effective pressure of 5 MPa. At 10 MPa and beyond, ductile behavior was observed with progressive increase of strain hardening at higher effective pressures. At 10 and 20 MPa effective pressures, porosity decreased to 0.39% and 1.2%, respectively, before reaching to the onset of shear-induced dilation (C*').

Under hydrostatic compression, the onset of pore collapse (P*) occured consistently at higher effective pressure (dry ~ 51.2 MPa; wet ~ 37.5 MPa) in GU1 than in GO (dry ~ 29.4 MPa; wet ~ 21.7 MPa). Our new P* data in dry and wet conditions indicate an almost equal water weakening in both GO and GU1 samples with around 27% strength reduction in both cases.

The failure envelopes for water-saturated GU and GO samples look qualitatively similar.

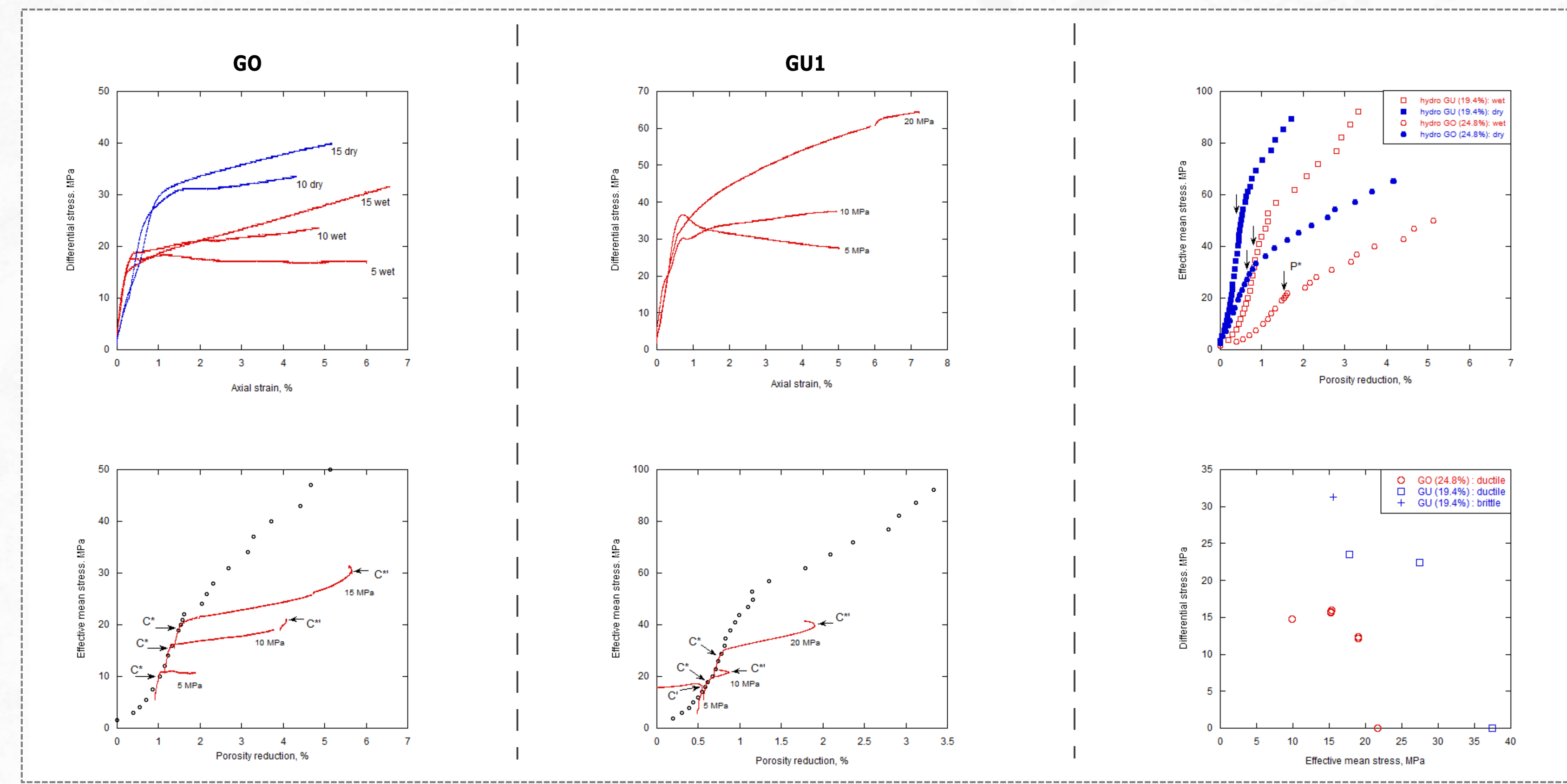

3.2. Hydrostatic and triaxial permeability

Under hydrostatic compaction, permeability decreased moderately in both GO and GU1 during the poroelastic stage and did not appear to decrease more significantly beyond the onset of pore-collapse (P*). At an effective pressure of 100 MPa, inelastic compaction resulted in a permeability reduction of a factor 15 in GO and a factor 4 in GU1, while respective porosity reduction was 7.8% and 2.5%.

Our new data on triaxial permeability shows in all cases modest variations, in agreement with previous studies on porous carbonates (Meng et al., 2019).

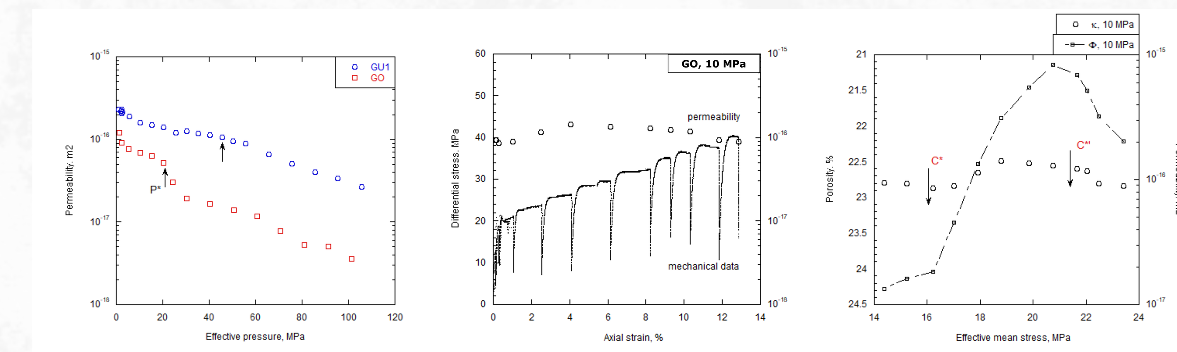

4. Microstructural observation

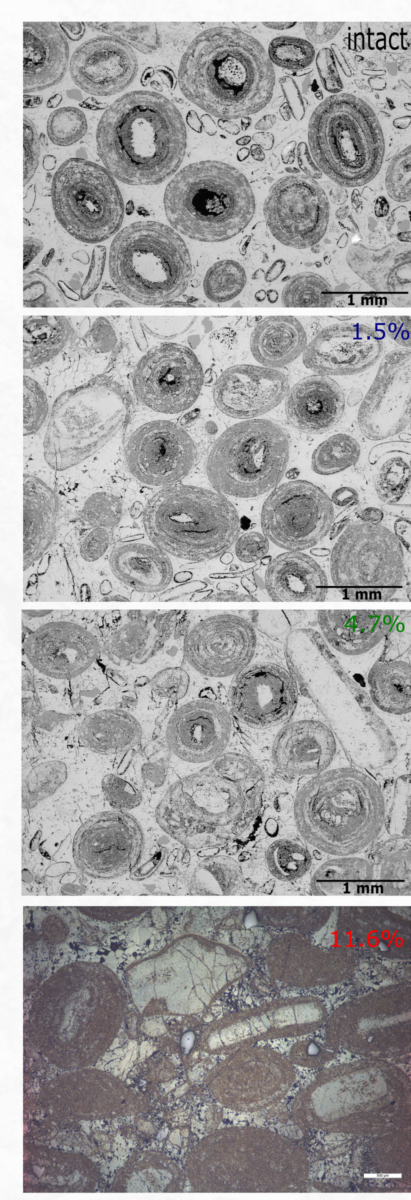

In samples of GO deformed at 10 MPa of effective pressure, stress-induced microcracking predominantly occurred within the sparite cement surrounding the grains, while intragranular cracks were mostly observed in the nonporous grains.

Quantitative characterisation of damage evolution (using stereologic technique) consistently revealed some increase in crack density and consequently, crack surface area, with progressive deformation.

Statistics on vertical and horizontal crack densities revealed comparable anisotropy in all deformed samples.

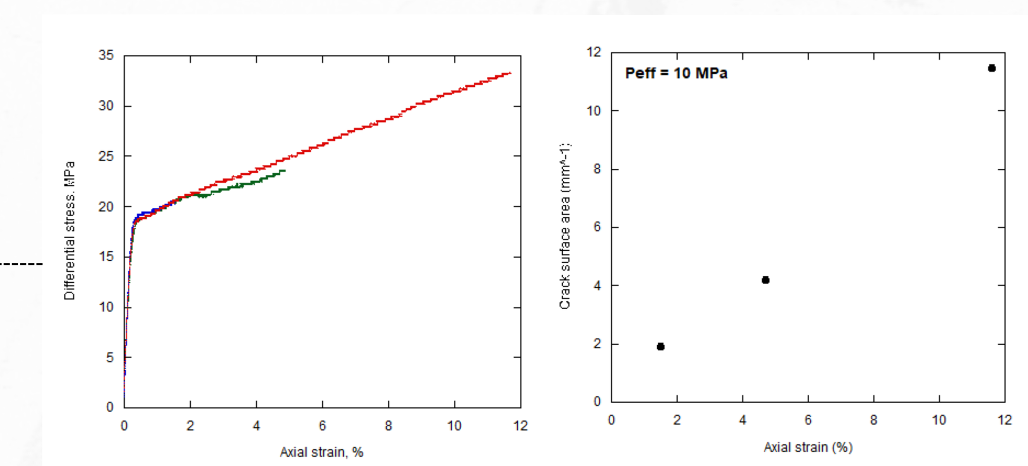

Sample	Axial strain (%)	Crack density for linear intercepts parallel to σ_1 $P_L^{\parallel}\,(\mathrm{mm}^{-1})$	Crack density for linear intercepts perpendicular to σ_1 $P_L^{\perp}\,(\mathrm{mm}^{-1})$	Crack surface area per unit volume $S_v(\mathrm{mm}^{-1})$
GO12	1.5%	0.339	1.131	1.923
GO2	4.7%	0.933	2.412	4.190
GO18	11.6%	2.014	6.747	11.463

5. Discussion

The empirical relation proposed by David et at. (1994) was used to analyze our permeability data under hydrostatic compaction.

$$k = k_0 \cdot \exp\left(-\gamma(P_{\text{eff}} - P_0)\right)$$

Pressure sensitivity exponent γ was found to increase beyond the onset of pore collapse in GU1 and not in GO.

The permeability of GO and GU1 limestones is lower than that of Indiana and Purbeck limestones, despite their smaller porosities. Under hydrostatic compaction, GO and GU1 exhibit a more pronounced reduction in permeability relative to their porosity loss compared to carbonates with dual-porosity systems, suggesting that micropores can exert greater control over permeability evolution.

Our permeability reduction with porosity are relatively small in comparison with corresponding changes in sandstones which can be up to 5 orders of magnitude.

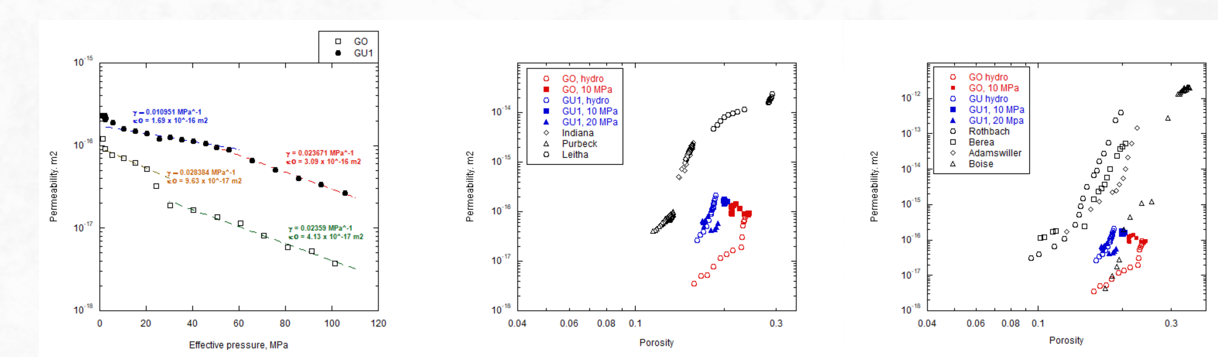

In comparison to the Oolite Blanche formation from Paris Basin, samples from the Grande Oolithe exhibit lower porosity, likely due to a higher degree of cementation. A higher permeability of Paris Basin can be due to the presence of mesopores and better connectivity among porous components such as ooids and pellets, as well as their connectivity.

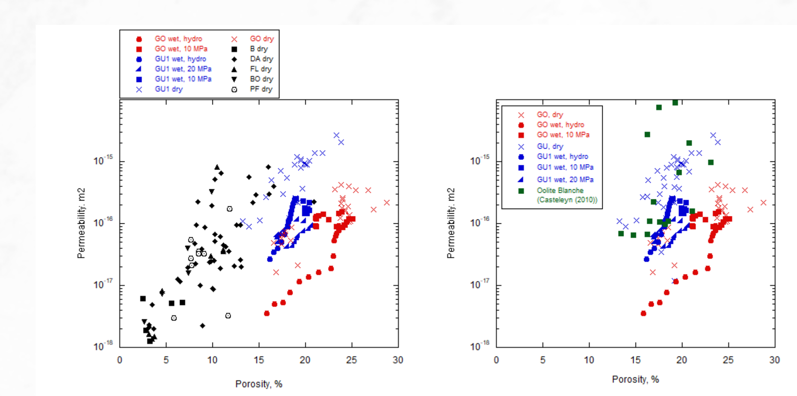

References

1. Zhu, W, Baud, P., & Wong, T.-f., 2010. Micromechanics of cataclastic pore collapse in limestone. Journal of Geophysical Research, 115, B04405. https://doi.org/10.1029/2009JB006610
2. Meng, F., Baud, P., Ge, H., Wong, T., 2019. The Effect of Stress on Limestone Permeability and Effective Stress Behavior of Damaged Samples. Journal of Geophysical Research: Solid Earth 124, 376–399. https://doi.org/10.1029/2018JB016526
3. Farquharson, J.I., Baud, P., Heap, M.J., 2017. Inelastic compaction and permeability evolution in volcanic rock. Solid Earth 8, 561–581. https://doi.org/10.5194/se-8-561-2017
4. Synthese documentaire sur la Grande Oolithe dans le département du Haut- Rhin, Decembre 1982, https://infoterre.brgm.fr/rapports/83-SGN-007-ALS
5. David, C., Wong, T.-F., Zhu, W., Zhang, J., 1994. Laboratory measurement of compaction-induced permeability change in porous rocks: Implications for the generation and maintenance of pore pressure excess in the crust. Pure and Applied Geophysics 143, 425–456. https://doi.org/10.1007/BF00874337
6. Zhang, R., Ning, Z., Yang, F., Zhao, H., Wang, Q., 2016. A laboratory study of the porosity-permeability relationships of shale and sandstone under effective stress. International Journal of Rock Mechanics and Mining Sciences 81, 19–27. https://doi.org/10.1016/j.ijrmms.2015.11.006
7. Casteleyn, L., Robion, P., Collin, P.-Y., Menéndez, B., David, C., Desaubliaux, G., Fernandes, N., Dreux, R., Badiner, G., Brosse, E., Rigollet, C., 2010. Interrelations of the petrophysical, sedimentological and microstructural properties of the Oolithe Blanche Formation (Bathonian, saline aquifer of the Paris Basin). Sedimentary Geology 230, 123–138. https://doi.org/10.1016/j.sedgeo.2010.07.003